Radio Science, Volume 36, Number 4, Pages 695–707, July/August 2001

SOMARE-99: A demonstrational field campaign for ultrahigh-resolution VHF atmospheric profiling using frequency diversity

Phillip B. Chilson,[1,2] Robert D. Palmer,[3] Andreas Muschinski,[4]
David A. Hooper,[1] Gerhard Schmidt,[5] and Hans Steinhagen[6]

Abstract. During May of 1999 the sounding system (SOUSY) VHF radar was operated in a demonstrational field campaign specially designed to test the applicability of range imaging (RIM) to radar studies of the atmosphere. The RIM technique utilizes frequency diversity to offer a novel method of improving radar range resolution over that which can be obtained with a conventional pulsed radar with the same bandwidth. During the field campaign, which is being called SOUSY Multifrequency Atmospheric Radar Experiment 1999 (SOMARE-99), the application of RIM on a VHF radar has been demonstrated. The data from SOMARE-99 are intended for investigating the dynamics and morphology of fine-scale vertical structures in the troposphere. This paper gives an overview of SOMARE-99 and provides some initial scientific results. A central and important result was obtained by comparing RIM-processed radar observations and data from radiosondes. Profiles of the vertical gradient of the generalized refractive index and the so-called RIM-enhanced echo power are found to bear similarities during one particular case, for which the radiosonde was located directly over the radar. Furthermore, a spectral analysis of these two parameters has provided evidence that RIM is successfully identifying multiple structures within the radar sampling volume with scales smaller than the conventional range resolution.

1. Introduction

The development of radar technologies for the study of the atmosphere has seen many exciting advances over the last decades, with many occurring in recent years [*Hocking*, 1997]. An underlying theme in these developments has been the quest for better temporal and spatial resolution measurements. Indeed, an understanding of many atmospheric phenomena, such as turbulent processes and dynamic instabilities, necessitate high-resolution measurements. The inherent layered structure of most of the atmosphere has led researchers to examine many methods that enable one to take better advantage of the available frequency content of a transmitted radar signals. By using conventional radar techniques, better range resolution is achieved by transmitting shorter pulses. The shorter pulses, of course, mean that less energy is available for exciting backscattering processes in the atmosphere and larger bandwidths are required. Although coding techniques are used to compensate for the former limitation, the latter remains a problem. Since hardware and frequency allocation restrictions limit the available amount of operational bandwidth, alternative methods using multiple-frequency observation strategies are being explored.

Each scientific technique has to undergo a process of maturity. The dual-frequency radar interferome-

[1]MRI Atmospheric Research Programme, Swedish Institute of Space Physics, Kiruna, Sweden.
[2]Now at the Cooperative Institute for Research in Environmental Sciences, University of Colorado-NOAA, NOAA Environmental Technology Laboratory, Boulder, Colorado.
[3]Department of Electrical Engineering and Center for Electro-Optics, University of Nebraska, Lincoln, Nebraska.
[4]Cooperative Institute for Research in Environmental Sciences, University of Colorado-NOAA, NOAA Environmental Technology Laboratory, Boulder, Colorado.
[5]Max-Planck-Institut für Aeronomie, Katlenburg-Lindau, Germany.
[6]Deutscher Wetterdienst, Meteorologisches Observatorium, Lindenberg, Germany.

Paper number 1999RS002308.
0048-6604/01/1999RS002308$11.00

try under the name of frequency domain interferometry (FDI) has already completed a series of steps in this process. The first step, scientific feasibility, is the demonstration of the technique as a useful tool for a particular application. For example, the practical application of this technique has been demonstrated by *Stitt and Bowhill* [1987] and *Kudeki and Stitt* [1987]. Afterward comes the test of experimental feasibility, or the technological and experimental realization [*Kudeki and Stitt*, 1990; *Palmer et al.*, 1990; *Chilson and Schmidt*, 1996]. Clearly, FDI has undergone the phase of producing new scientific results, as shown by *Chilson et al.* [1997] and *Muschinski et al.* [1999].

Despite its accomplishments, FDI is reaching the limits of its development, and we are beginning to see the advent of new multifrequency methods that utilize two or more radar carrier frequencies. One such technique, known as range imaging (RIM) [*Palmer et al.*, 1999], offers a very promising means of probing the atmosphere. Although RIM is still in the early phases of development, we envision that it will have an impact on remote measurements of atmospheric phenomena.

We have conducted a week-long experimental campaign using the sounding system (SOUSY) VHF radar in which four-frequency RIM was completed under the name of SOUSY Multifrequency Atmospheric Radar Experiment 1999 (SOMARE-99). In this paper, we discuss the application of RIM techniques to the study of fine-scale atmospheric scattering layers. We provide an overview of the campaign and some initial scientific results. We mainly focus on validation of RIM by comparing its results with meteorological sounding data. A description of how the technique has been realized on the SOUSY VHF radar is given in our companion paper [*Palmer et al.*, this issue]. *Muschinski et al.* [2001] report on diurnal variations seen in frequency spectra and discuss the 1 hour variances of the surface pressure and the vertical wind aloft.

2. Description of the Experiment

During May 1999 the multinational experimental campaign SOMARE-99 was conducted in Germany; it was specially designed to test the applicability of RIM to radar studies of the atmosphere. The data from the experiment will be used to investigate the dynamics and morphology of fine-scale vertical refractivity structures in the troposphere. The primary instrument used in the campaign was the SOUSY VHF radar located in the Harz Mountains in Germany. To achieve ultrahigh-resolution measurements, the radar was operated in a multifrequency mode. To complement the radar measurements, the Deutscher Wetterdienst (DWD) launched a series of radiosondes 25 km to the west of the SOUSY radar, which were monitored by the DWD tracking radar. Additionally, a network of four high-resolution pressure sensors was operated in the vicinity of the SOUSY radar site. A description of these instruments is given in sections 2.1 and 2.2 and Table 1 gives their locations. The relative locations are also shown in Figure 1.

2.1. SOUSY VHF Radar

The SOUSY VHF radar operates at a nominal frequency of 53.5 MHz and is capable of transmitting a peak power of 600 kW. The radar uses a phased array antenna that consists of 196 Yagi aerials and has dimensions of 72 m × 72 m. The main beam of the array has a one-way half-power beam width of 5° when directed vertically and can be steered over a continuous range of pointing angles. A more detailed

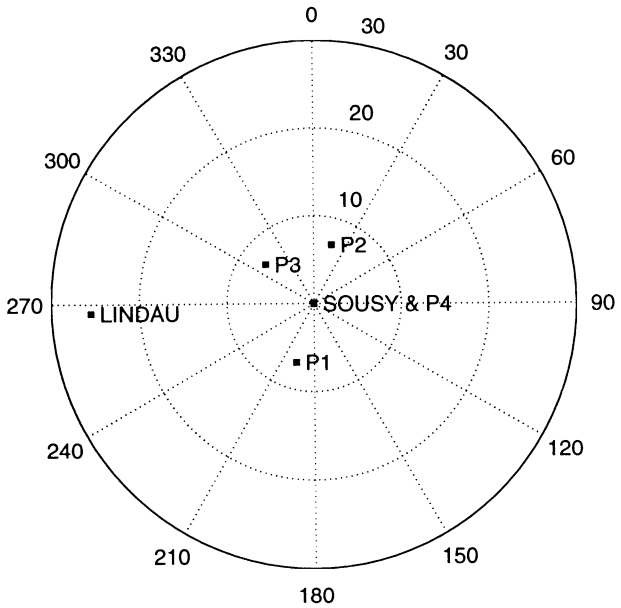

Figure 1. Map showing the locations of the radiosonde launch site (Lindau) and the four pressure sensors relative to the SOUSY VHF radar. The pressure sensor sites are Bartolfelde (P1), St. Andreasberg (P2), Sieber (P3), and the SOUSY VHF radar site (P4). Range markers of 10, 20, and 30 km are shown.

Table 1. Experimental Site Locations

Name	Coordinates	Height, m
SOUSY VHF radar	51.66°N, 10.49°E	333
Radiosonde launch site (Lindau)	51.65°N, 10.12°E	142
Pressure sensor 1 (Bartolfelde)	51.60°N, 10.46°E	264
Pressure sensor 2 (St. Andreasberg)	51.72°N, 10.52°E	741
Pressure sensor 3 (Sieber)	51.70°N, 10.41°E	357
Pressure sensor 4 (SOUSY radar)	51.66°N, 10.49°E	333

description of the radar is given by *Czechowsky et al.* [1984] and *Schmidt et al.* [1979].

The SOUSY radar was operated during SOMARE-99 from 1445 UT on May 24 till 1539 UT on May 28, 1999. A description of the operating parameters of the radar during the experiment is presented in our companion paper [*Palmer et al.*, this issue]. Note that some data gaps resulted from technical problems with the radar.

2.2. Supporting Instruments

The DWD supported SOMARE-99 by launching a series of radiosondes (see Figure 1). A total of 26 radiosondes were launched every 3 hours during the period of May 25 at 1200 UT through May 28 at 1500 UT. Pressure, temperature, and relative humidity data from the radiosondes were recorded every 1.3 s, which on the basis of typical ascent rates, corresponds to an altitude sampling interval of ~7-8 m. These data are used in section 4 to interpret the radar returns from the SOUSY radar.

The pressure sensor has a resolution of 0.1 hPa and an inaccuracy (standard deviation) of ±0.5 hPa. The temperature sensor has a resolution of 0.1 K and an inaccuracy of (standard deviation) of ±0.2 K. The humidity sensor has a resolution of 1% and an inaccuracy (standard deviation) of ±2%. Further details are given by *Antikainen and Hyvönen* [1983].

The radiosondes were positioned by the DWD 9375 MHz tracking radar. These data were provided every 10 s and were used to estimate the horizontal wind vector. All available data were processed by the DWD to produce 10 s resolution data of altitude, pressure, temperature, relative humidity, wind speed, wind direction, and ascent rate during the first during the first 5 min of the ascent and 20 s resolution data thereafter.

A network of four high-resolution pressure sensors was placed at various locations near the SOUSY radar as shown in Figure 1. One pressure sensor was located at the radar site. The other three sensors were located in a noncoplanar array around the radar. See Table 1 for the exact coordinates of the sensors. The distances of the pressure sensors from the SOUSY radar were 6.73, 7.22, and 7.23 km. The resolution of all pressure sensors is approximately 0.01 hPa, and they have an inaccuracy (standard deviation) of ~0.02 hPa. *Muschinski et al.* [2001] report the diurnal variation of frequency spectra and 1 hour variances of the surface pressure and the vertical wind aloft in the context of boundary layer convection and of gravity wave motion in the free troposphere.

3. Data Overview

During SOMARE-99 a high-pressure system dominated over the SOUSY radar site, which led to generally clear, stable atmospheric conditions. An upper level trough associated with an Iceland low moved eastward from Ireland (May 24, 1200 UT) over the North Sea (May 25, 1200 UT) to the Baltic Sea (May 26, 1200 UT). On May 24, 1200 UT, westerly winds in the polar front jet stream over the North Sea reached 50 m s^{-1}. The SOUSY VHF radar site was at the southern boundary of the upper level polar frontal zone during these 3 days. Therefore the strong winds in the jet stream were not seen with the radar, except on May 25 around noon: when the meridional gradient of the geopotential height of the 300 hPa surface above the radar site went through a maximum, upper level westerly winds of up to 30 m s^{-1} were observed with the radar. With the exception of the passage of the upper level trough on May 25, the meteorological situation the radar site was characterized by anticylonic flow. A local thunderstorm developed on May 28 in the near vicinity of the radar. A power outage associated with the thunderstorm resulted in termination of the experiment slightly earlier than scheduled.

3.1. Radar Data

The general procedure for analyzing the SOUSY VHF radar data is given in our companion paper [*Palmer et al.*, this issue]. We adopt a somewhat different method of representing the RIM data to that given in *Palmer et al.* [this issue]. They shade the range brightness profiles with the logarithm of the echo power (see Figures 2, 3, 5, and 6 of *Palmer et al.* [this issue]), which is highly useful for visualizing the thickness and dynamics of individual scattering layers. However, this method does not reproduce what a higher-resolution radar would actually measure. We begin by calculating $B(r_I, f)$ using the modified form of W_r [*Palmer et al.*, this issue]. The resulting range brightness is then normalized such that the sum of $B(r_I, f)$ within each range gate equals unity. Then we used a four-element running mean characterized by a zero phase shift to filter the range brightness. That is, the resulting range brightness has a resolution of approximately 20 m. This profile of the range brightness was multiplied by the profile of the conventional echo power, P, in linear units. We refer to the resulting RIM-enhanced echo power as P_{RIM}. Examples of data processed using this method are shown in section 4.

3.2. Radiosonde Data

We now consider the data collected with the radiosonde soundings. If we assume that the radar sampling volume is filled with statistically isotropic and homogeneous refractive index irregularities and that the Bragg scale of the radar lies within the inertial subrange, then the volume reflectivity is simply given by [*Tatarskii*, 1961; *Atlas et al.*, 1966; *Ottersten*, 1969]

$$\eta = c_{\mathrm{TO}} C_n^2 \lambda^{-1/3}, \tag{1}$$

where c_{TO} is the Tatarskii-Otterson coefficient (0.379) [*Muschinski*, 1997], C_n^2 is the refractive index structure parameter, and λ is the radar wavelength. The refractive index structure parameter can be expressed as

$$C_n^2 = a^2 L_o^{4/3} M^2, \tag{2}$$

where a is a physical constant; L_o is the outer scale of Kolmogorov-type inertial range turbulence, and M is the vertical gradient of the generalized refractive index [*Atlas et al.*, 1966; *Ottersten*, 1969]. We can can express M^2 as

$$M^2 = (M_d + M_w)^2, \tag{3}$$

where M_d and M_w are the dry and the wet components of M, respectively, and are given by

$$M_d = -7.76 \times 10^{-7} \frac{p}{T^2} \left(\frac{\partial T}{\partial z} + \Gamma \right), \tag{4}$$

$$M_w = 6.05 \times 10^{-3} \frac{p}{T^2} \frac{\partial q}{\partial z}. \tag{5}$$

In (4) and (5), p is pressure, T is temperature (not potential temperature), z is height, q is the specific humidity, and Γ is the dry adiabatic lapse rate. SI units are assumed.

The Fresnel reflection and scatter as well as the Bragg scatter from isotropic turbulence can contribute to echo power at VHF [*Gage and Balsley*, 1980; *Röttger*, 1980]. Since we are primarily considering data from the vertically pointing radar beam, the echo powers being discussed here could contain contributions from Bragg scatter from turbulence and Fresnel reflection and scatter from thin laminae in the atmosphere. Although the underlying physics is completely different, both the Bragg scatter and the Fresnel reflection and scatter are proportional to $(M_d + M_w)^2$, albeit at different scales, for example, as discussed by *Gage* [1990, and references therein].

We have generated profiles of M^2 from (3) using the 1.3 s radiosonde data. Height and pressure information from the 10 s resolution, DWD-processed radiosonde data were used to match height values to the pressure values from the 1.3 s resolution data. The height, pressure, and temperature data were then forced onto a grid having a vertical spacing of 5 m by using linear interpretation. Then the data were filtered by using a five-element running mean characterized as having zero phase shift. Finally, values of M_d and M_w were calculated at each 5 m grid point using data over a 45 m range. That is, values of p and T were averaged over 45 m, and the derivatives in (4) and (5) were calculated by using a linear fitting routine over the 45 m height interval.

Plate 1 provides an overview of atmospheric conditions during SOMARE-99 as observed by the SOUSY VHF radar, the radiosondes, and the surface-level pressure sensor located at the radar site. Note that the logarithm of M^2 has been plotted so as to better correspond to the radar echo power P, which is expressed in decibels. Note also that a diurnal variation is present in each of the three parameters. Furthermore, some of the coarse features in the range-time-intensity (RTI) plot of P are additionally found

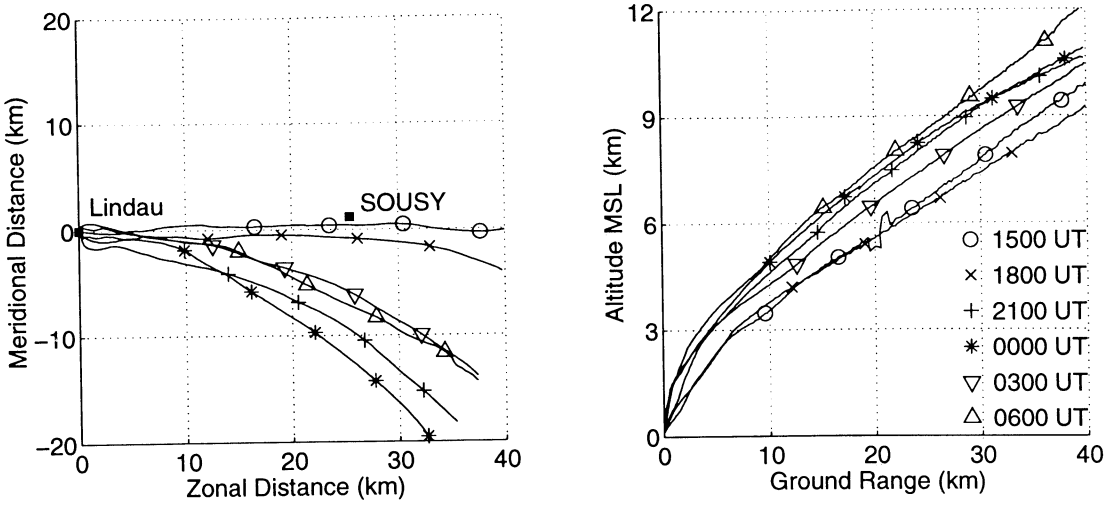

Figure 2. Locations of six of the radiosondes launched during SOMARE-99. The traces are for 1500 UT (circles), 1800 UT (crosses), and 2100 UT (pluses) on May 25 and 0000 UT (asterisks), 0300 UT (down triangles), and 0600 UT (up triangles) on May 26.

in the RTI plot of M^2. The profiles of M^2 have only been collected every 3 hours and the sondes require ~30 min to reach an altitude of 8 km. Since the radar and radiosonde measurements have been collected in Eulerian and Lagrangian frames, respectively, some differences are certainly expected. However, the similarities in the RTI plots warrant a closer comparison between the two quantities. Such a comparison is presented in section 4.

4. Radar Returns from Atmospheric Scattering Layers

Over the last several decades, many targeted observational campaigns and theoretical studies have been completed to investigate the mechanisms responsible for the scatter and reflection of radio waves by the atmosphere. Although much has been learned from these studies, many aspects of the governing processes remain unclear. For example, why are atmospheric echoes measured with VHF radars sometimes aspect sensitive [*Gage and Green*, 1978], and why is the aspect sensitivity not as strong at UHF? The atmosphere has been shown to be replete with fine-scale structure in the vertical extent [*Dalaudier et al.*, 1994; *Luce et al.*, 1995; *Eaton et al.*, 1995; *Muschinski and Wode*, 1998]. So observational atmospheric data having ultrahigh vertical resolution are essential to complete a consistent picture of atmospheric scattering processes.

4.1. Comparison of Radar and Radiosonde Data

As shown in our companion paper [*Palmer et al.*, this issue], the prevailing wind was westerly (toward the east) during the beginning of the radiosonde launch sequence. Considering the location of the launching site (Figure 1), under these conditions the balloons would be carried roughly over the SOUSY VHF radar site. The trajectories and altitudes of 6 of the 26 sondes are presented in Figure 2. Shown in Figure 2 are the radiosondes corresponding to the period May 25, 1500 UT, to May 26, 0600 UT. The first radiosonde, the one launched on May 25 at 1200 UT, is not shown because there were mechanical problems with the tracking radar.

The radiosonde launched at 1500 UT on May 25 passed closest to the radar at site of the six sondes presented in Figure 2. Indeed, it passed the closest to the radar site of all the 26 radiosondes launched. Therefore we will focus on this particular case when comparing radar and radiosonde data. The radiosonde is within the sampled height range of the radar from ~1507 UT till 1523 UT. The height of the radiosonde at the time it passes closest to the radar site is ~7 km.

A method of using RIM processed data to generate RIM-enhanced echo power P_{RIM} data was described in section 3. RTI plots of both the conventional echo power and P_{RIM} for the period 1400 UT to 1600 UT

on May 25 are presented in Plate 2. Note that the radiosonde can actually be seen in the RTI plots at an altitude and time of approximately 7.5 km and 1528, respectively. The plots provide an illustration of the suitability of RIM for studies of the atmosphere. It is clear that the P_{RIM} values shown in the lower panel reveal more vertical structure than is seen in the data for the conventional echo power P. Although the RTI plot of P_{RIM} is impressive, two obvious questions must be asked at this point: Are the structures revealed in the RIM echo power representative of what one might expect to observe, and are they consistent with the local atmospheric conditions?

To answer the first question, we consider results from other high-vertical-resolution radar observations. Frequency-modulated continuous wave radars are capable of identifying atmospheric structures with a resolution of approximately 1 m [*Richter*, 1969; *Gossard*, 1990; *Eaton et al.*, 1995]. Images from these radars have been used to identify a host of small-scale atmospheric structures such as Kelvin-Helmholtz billows, cells in the convective boundary layer, and small-amplitude buoyancy waves. Turning to pulsed Doppler radar, *Rüster et al.* [1998] presented results from several observations in which the SOUSY VHF radar was operated with a range resolution of only 75 m. Their Figures 1 and 7 reveal structures similar to those shown in Plate 2 of this paper. Other examples of high-vertical-resolution radar measurements are given by *Sato and Woodman* [1982], *Cho et al.* [1996], and *Ierkic et al.* [1990]. The in situ measurements reported by *Dalaudier et al.* [1994] and *Muschinski and Wode* [1998] further demonstrate the propensity of the atmosphere to exhibit fine-scale vertical structuring under favorable conditions.

Average profiles of the conventional echo power and RIM-enhanced echo power have been generated from a series of nine contiguous multiple-frequency (MUFR) records. See our companion paper for a description of the MUFR records [*Palmer et al.*, this issue]. The time of the first MUFR record used in the average is chosen to correspond to the time the radiosonde has been in flight for 15 min (a height of ~4 km). At the end of the averaging period the radiosonde has reached a height of ~6.5 km. The resulting averaged profiles of P_{RIM} and P together with the profile of M^2 estimated from the radiosonde data

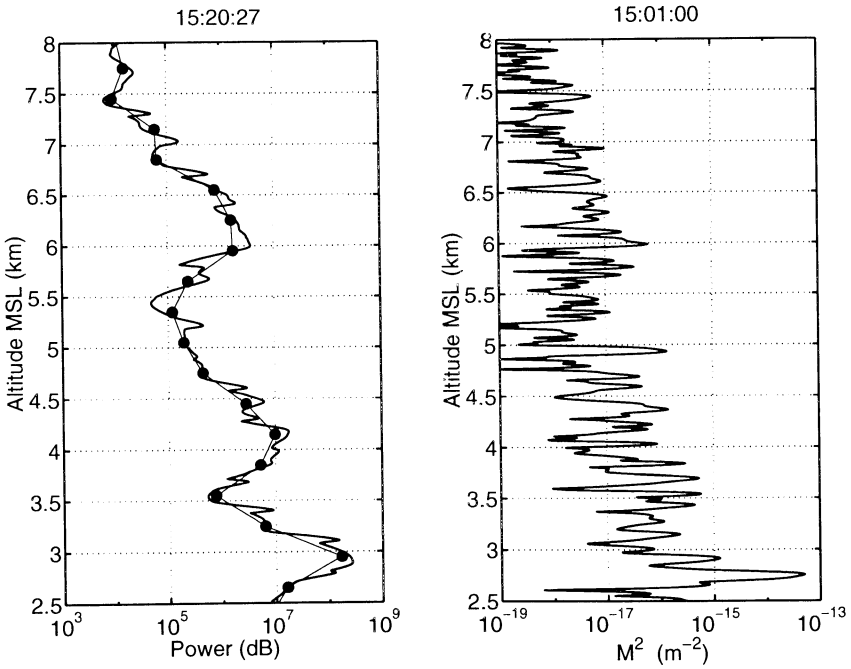

Figure 3. (left) Height profiles of the conventional echo power (thin solid line with solid circles) and RIM-enhanced echo power (thick solid line). (right) Profile of the vertical gradient of the generalized refractive index squared. The profile was calculated using the 1.3 s data from a radiosonde launched at 1500 UT.

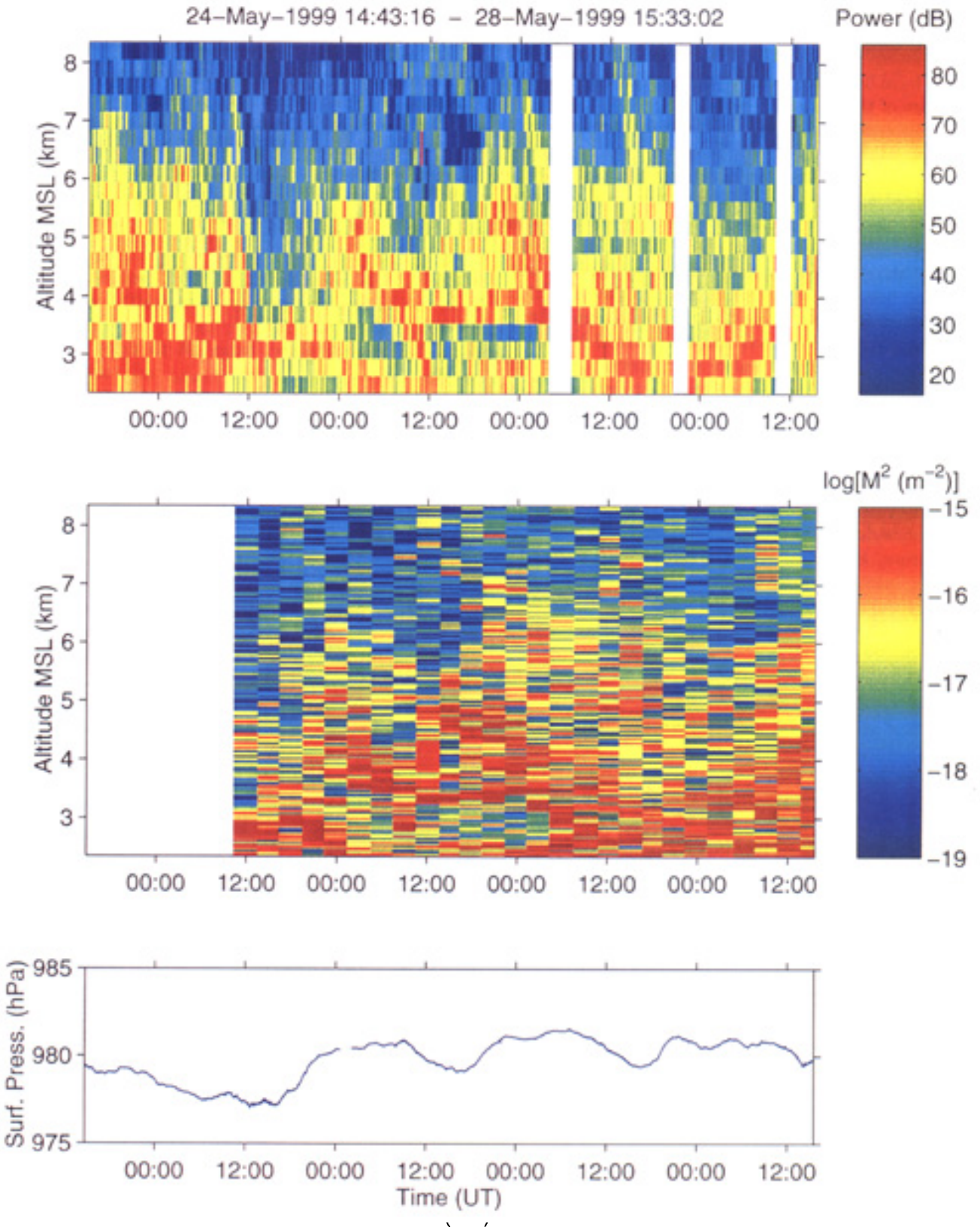

Plate 1. Overview plot of the conditions during SOMARE-99. (top) Echo power measured using the vertical beam of the DBS cycle. Data gaps are indicated as vertical white stripes. (middle) Calculated values of M^2. The first of the 26 radiosondes was launched at 1200 UT on May 25. (bottom) Surface pressure measured at the radar site.

are shown in Figure 3. Note that the power profiles have been range corrected by multiplying by the square of the altitude.

This comparison suggests that the features shown in the RIM-enhanced echo power are truly geophysical in origin. The finer-scale features observed in the profile of M^2 are obviously lost at the resolution of the conventional echo power. We admit that one should be cautious when comparing single profiles. More radar data and radiosonde data are presented below using a spectral analysis. We note that *Tsuda et al.* [1988] present data from a comparitive study of radar echo power and estimates of M^2 based on upper tropospheric and stratospheric observations made in Japan. They report excellent agreement between profiles of the normalized signal-to-noise ratio in the vertical direction (after compensating for range-squared effects) and M^2.

Next, we consider estimates of the humidity and Brunt-Väisälä frequency from the 10 s resolution radiosonde data. As earlier, the data for pressure, temperature, and humidity were forced onto a grid by using linear interpretation, but this time with a vertical spacing of 50 m. We used these data to calculate the square of Brunt-Väisälä frequency as given by

$$\omega_B^2 = \frac{g}{\theta}\frac{d\theta}{dz}, \tag{6}$$

where θ is the potential temperature and g is the gravitational acceleration. In this study, the value of ω_B^2 has been calculated by using an altitude step of 300 m. Many examples in the literature [e.g., *Hooper and Thomas*, 1998] show that ω_B^2 and M_d^2 are closely related and, thus, related to the received echo power when the atmosphere is relatively dry.

A useful parameter when examining atmospheric stability is the degree of turbulence. Although a measure of atmospheric turbulence can be obtained through estimates of the width of the Doppler spectrum, many factors besides atmospheric turbulence can lead to the broadening of Doppler spectra. These include beam broadening, shear broadening, and gravity wave broadening. A measure of turbulent broadening can be calculated from the observed Doppler spectral width by using

$$\sigma_{\text{turb}}^2 = \sigma_{\text{obs}}^2 - \sigma_{\text{beam}}^2 - \sigma_{\text{shear}}^2 - \sigma_{\text{wave}}^2, \tag{7}$$

where σ_{obs}^2 is the observed spectral width and σ_{turb}^2, σ_{beam}^2, σ_{shear}^2, and σ_{wave}^2 are the turbulence, beam, shear, and gravity wave contributions to the spectral width, respectively [*Nastrom and Eaton*, 1997, and references therein]. Of these, beam-broadening contributions typically dominate. Therefore we neglect the shear and gravity wave contributions to spectral broadening in this treatment of the data. An expression for beam broadening can be written as

$$\sigma_{\text{beam}}^2 = v_h^2 \left(\frac{\theta_1}{2}\right)^2 \frac{1}{2.76}, \tag{8}$$

where v_h is the magnitude of the horizontal wind and θ_1 is the half-power one-way beam width [*Hocking*, 1983].

In Figure 4 we show, from left to right, height profiles of P_{RIM}, σ_{obs} and σ_{turbc}, ω_B^2, and relative humidity. Missing values of the corrected spectral width correspond to regions in which σ_{beam} were larger than σ_{obs}. Some features are immediately discernible in Figure 4: A layer of high atmospheric stability indicated by enhanced values of ω_B^2 is present at an altitude of 3 km, which corresponds to the lower boundary of the strong horizontal wind. See our companion paper [*Palmer et al.*, this issue]. This layer imposes an upper boundary on the lower level atmospheric humidity. At altitudes of 4.3 and 5.8 km, regions of enhanced values of ω_B^2 correspond to minima in the values of spectral width and maxima in the echo power.

The altitudes of the local maxima in ω_B^2, namely, 4.3 and 5.8 km, also correspond to the regions where the calculated value of σ_{beam} overcompensates for beam broadening. An earlier study of jet streams using the SOUSY radar showed (8) to be a reliable means of removing beam broadening from Doppler spectral widths [*Yoe et al.*, 1994]. Note that *Yoe et al.* [1994] used longer averaging times in their estimates than are being considered here. What mechanism could account for the overcompensation of spectral width due to beam broadening in this case? Although not shown, the ratios of the echo power from the vertical and off-vertical beams in the Doppler beam swinging (DBS) cycle for the data presented in Figure 4 show maxima at altitudes where the over compensation has occurred. That is, the atmosphere is aspect sensitive in these regions. *Hocking et al.* [1990] have shown that the effective radar beam width can be reduced when the atmosphere is aspect sensitive. Therefore the value of θ_1 of 5° used in calculating σ_{beam} is probably too large. The effects of the reduced value of θ_1 become increasingly relevant with an increase in the magnitude of the horizontal

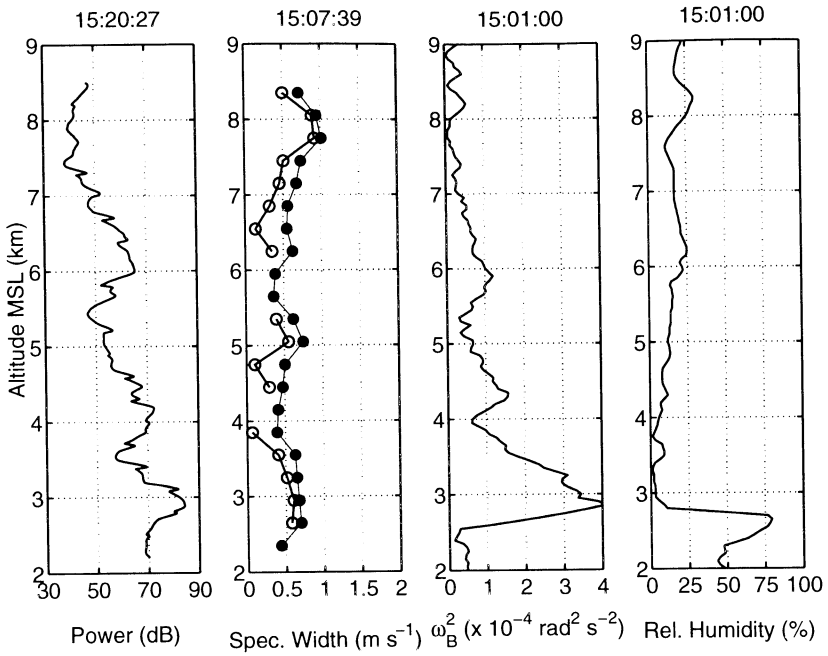

Figure 4. Height profiles from left to right of P_{RIM}, beam-broadening corrected (open circles) and uncorrected (solid circles) spectral widths, square of the Brunt-Väisälä frequency, and relative humidity

wind. Refer to our companion paper for wind data [*Palmer et al.*, this issue].

4.2. Spectral Analysis of P_{RIM} and M^2

So far we have only considered a small portion of the SOMARE-99 data set. To obtain a more statistical picture of how the radar and radiosonde data compare, we next present a spectral analysis study of P_{RIM} and M^2 profiles using data from the six radiosondes presented in Figure 2. Before performing the spectral analysis the profiles of P_{RIM} and M_d^2 were preprocessed as described below.

Average profiles of the RIM-enhanced echo power were generated from a series of nine contiguous MUFR records as described in section 4.1. For the spectral analysis, only data from the altitude range between 5 and 7 km were considered. The resulting profiles were range corrected by multiplying by the square of the altitude. To focus on the small-scale features in the profiles, the data for P_{RIM} and M^2 were filtered in height through a sixth-order band-pass Butterworth filter. The 3 dB points for the filter correspond to length scales of 70 and 1100 m. Then, autospectra were calculated as a function of wavenumber from the resulting data.

The self-normalized autospectra of P_{RIM} and M^2 for the times corresponding to the six radiosonde launches are shown in Figure 5. Before calculating the spectra the profiles P_{RIM} and M^2 were weighted with a Hanning window, which reduces possible spectral leakage but also slightly widens the spectral peaks. Additionally, the magnitude of Butterworth filter's frequency response is shown in the lowermost panels. The dashed vertical lines indicate the wavenumbers representing scale sizes of 300 m ($k_z/2\pi = 3.33 \times 10^{-3}$ m^{-1}). We note that for a conventional range resolution of 300 m the smallest detectable scale sizes would be twice the sampling interval, or 600 m ($k_z/2\pi = 1.67 \times 10^{-3}$ m^{-1}). There are clearly peaks in the RIM data corresponding to vertical structures smaller than 300 m.

Based on the radiosonde trajectories shown in Figure 2, we could expect the best agreement between the the autospectra of P_{RIM} and M^2 for the radiosonde launched at 1500 UT. Recall that these spectra were calculated from data obtained by completely independent instruments, namely, the SOUSY VHF radar and radiosondes. Therefore we should not hope for the spectra for the radar and radiosonde data to be the same. However, if the different observations are detecting similar vertical scaling in the

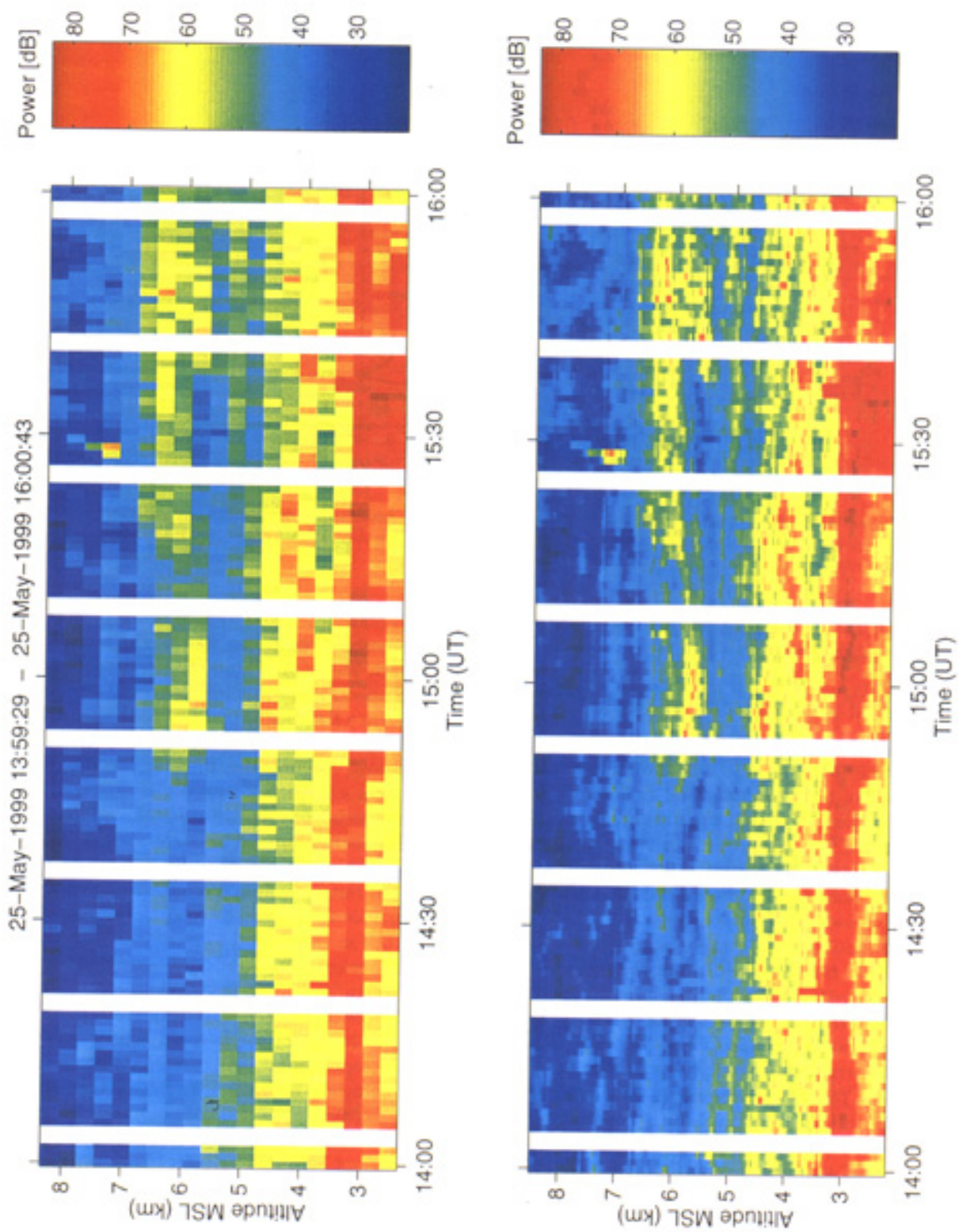

Plate 2. RTI plot of (top) the conventional echo power and (bottom) the RIM-enhanced echo power corresponding to the radiosonde launch time of 1500 UT on May 25.

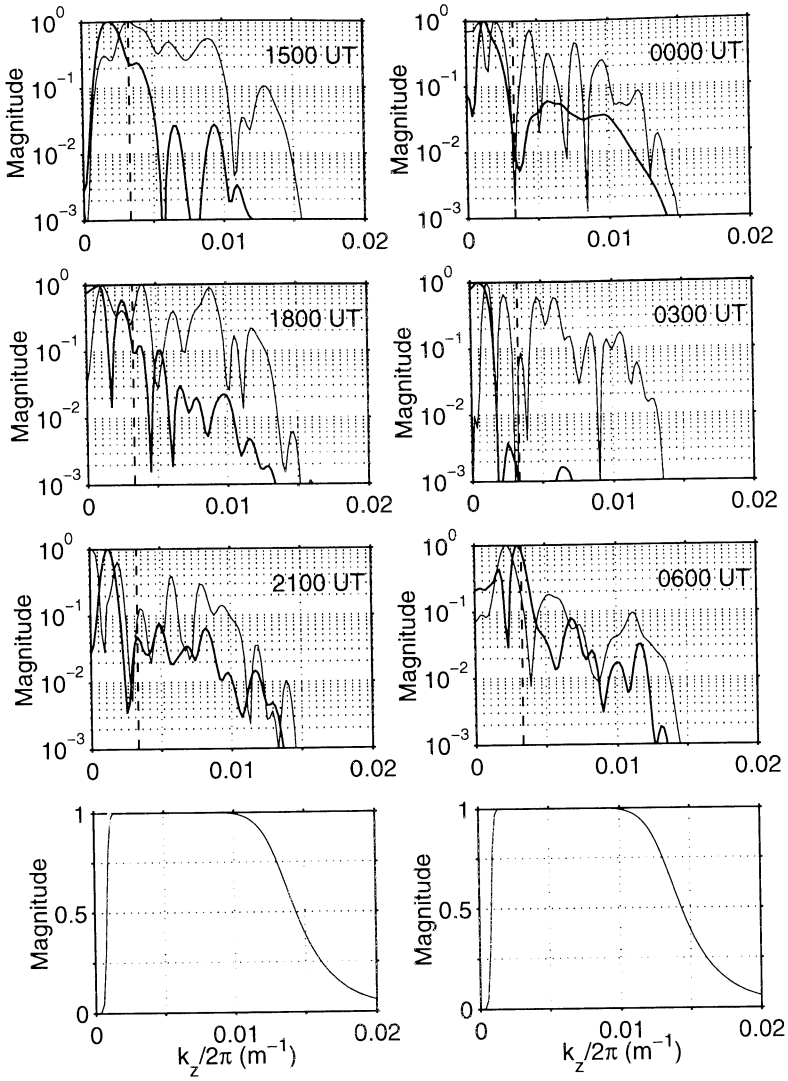

Figure 5. Autospectra calculated from the vertical profiles of P_{RIM} and M^2 for the times corresponding to the six radiosondes shown in Figure 2. The spectra for P_{RIM} and M^2 are given by thick and thin lines, respectively. Also shown is the magnitude of filter's frequency response is shown in the lowermost panels. See text for details.

atmosphere, then it may be possible to find spectral peaks having the same wavenumbers. We begin by examining the spectra for the data collected around 1500 UT. The spectral peaks for the two data sets corresponding to larger vertical scales correlate rather well. At least there appears to be a counterpart in the P_{RIM} data for every spectral peak in M^2 down to scale sizes of ~100 m. We note that one should be careful interpreting the first peak (smallest wavenumber) since it is probably shaped by the filter.

We now consider the spectra for the times of the other five radiosonde launches. In particular, we are interested in the spectra for the 1800 UT case, since this radiosonde also passed near the radar site. The spectral peaks for the P_{RIM} and M^2 do seem to match for smaller wavenumbers, but only to scale sizes just under 300 m. The spectra do not appear to agree for larger wavenumbers. The other four cases, which correspond to radiosondes that were further from the radar site, do not demonstrate much agreement.

5. Conclusions

An application of RIM on a VHF radar has been demonstrated within the context of SOMARE-99. The flexible SOUSY radar is well suited to multiple-frequency measurements, as has been demonstrated using FDI [*Chilson and Schmidt*, 1996; *Chilson et al.*, 1997; *Muschinski et al.*, 1999]. Whereas FDI measurements use a single frequency pair, the SOMARE-99 radar observations used four, phase-calibrated frequencies within a 500 kHz spacing [*Palmer et al.*, this issue]. One of the underlying objectives of SOMARE-99 was to test the applicability of RIM to radar studies of the atmosphere. However, investigating the dynamics and morphology of fine-scale vertical structures in the troposphere was certainly also important.

A central and important result of the present study was obtained by comparing RIM-processed radar observations and data from radiosondes. Profiles of the vertical gradient of the generalized refractive index M^2 and the RIM-enhanced echo power P_{RIM} are shown to be similar for a case when the radiosonde passed near the radar site. Unfortunately, the radiosonde was closest to the radar within a time and height range for which the radar echo power was not very strong. Nevertheless, the results suggest that the vertical structures seen using the RIM technique are geophysical and not an artifact of processing.

It is usually difficult to compare results from different observational techniques. This is especially true for the data presented here since the radar and radiosondes were making Eulerian and Lagrangian measurements, respectively. Furthermore, the two instruments are inherently collecting data on different spatial and temporal scales. However, the spectral analysis of P_{RIM} and M^2 has provided evidence that the RIM is successfully identifying structures in the radar data with verticl scale sizes smaller than the conventional range resolution.

The results of this paper and those of *Muschinski et al.* [2001] and *Palmer et al.* [this issue] have only begun to exploit the potentials of radar RIM and to capitalize on the information contained in the SOMARE-99 data set. It remains to study dynamical effects and atmospheric motions using the RIM data: one of the objectives of the SOMARE-99 experiment. Additional results from the ongoing analysis of SOMARE-99 will be presented in the future.

Acknowledgments. SOMARE-99 was jointly supported by the Max-Planck-Institut für Aeronomie, Katlenburg-Lindau, Germany; the National Oceanic and Atmospheric Administration's Environmental Technology Laboratory, Boulder, Colorado; the Swedish Institute of Space Physics, Kiruna, Sweden; the Deutscher Wetterdienst, Offenbach, Germany; and the Deutscher Wetterdiensts Meteorologisches Observatorium, Lindenberg, Germany P.B.C. and D.A.H. were supported by the Environment and Space Research Institute (MRI) in Kiruna, Sweden. R.D.P. was supported by the Division of Atmospheric Sciences of the National Science Foundation (United States) through grant ATM 99-08616.

References

Antikainen, V., and V. Hyvönen, The accuracy of Vaisala RS80 radiosonde, paper presented at 5th Symposium of Meteorological Observations and Instruments, Am. Meterol. Soc., Toronto, 1983.

Atlas, D., K. R. Hardy, and K. Naito, Optimizing the radar detection of clear air turbulence, *J. Appl. Meteorol.*, *5*, 450–460, 1966.

Chilson, P. B., and G. Schmidt, Implementation of frequency domain interferometry at the SOUSY VHF radar: First results, *Radio Sci.*, *31*, 263–272, 1996.

Chilson, P. B., A. Muschinski, and G. Schmidt, First observations of Kelvin-Helmholtz billows in an upper level jet using VHF frequency domain interferometry, *Radio Sci.*, *32*, 1149–1160, 1997.

Cho, J. Y. N., R. F. Jurgens, and M. A. Slade, High-resolution stratospheric dynamics measurements with the NASA/JPL Goldstone Solar System Radar, *Geophys. Res. Lett.*, *23*, 1909–1912, 1996.

Czechowsky, P., G. Schmidt, and R. Rüster, The mobile SOUSY Doppler radar: Technical design and first results, *Radio Sci.*, *19*, 441–450, 1984.

Dalaudier, F., C. Sidi, M. Crochet, and J. Vernin, Direct evidence of "sheets" in the atmospheric temperature field, *J. Atmos. Sci.*, *51*, 237–248, 1994.

Eaton, F. D., S. A. McLaughlin, and J. R. Hines, A new frequency-modulated continuous wave radar for studying planetary boundary layer morphology, *Radio Sci.*, *30*, 75–88, 1995.

Gage, K. S., Radar observations of the free atmosphere: Structure and dynamics, in *Radar in Meteorology*, edited by D. Atlas, pp. 534–565, Am. Meterol. Soc., Boston, Mass., 1990.

Gage, K. S., and B. B. Balsley, On the scattering and reflection mechanisms contributing to clear air radar echoes from the troposphere, stratosphere, and mesosphere, *Radio Sci.*, *15*, 243–257, 1980.

Gage, K. S., and J. L. Green, Evidence for specular reflection from monostatic VHF radar observations of the stratosphere, *Radio Sci.*, *13*, 991–1001, 1978.

Gossard, E. E., Radar research on the atmospheric boundary layer, in *Radar in Meteorology*, edited by D. Atlas, pp. 477–527, Am. Meterol. Soc., Boston, Mass., 1990.

Hocking, W. K., On the extraction of atmospheric turbulence parameters from radar backscatter Doppler spectra, part I; Theory, *J. Atmos. Terr. Phys.*, *45*, 89–102, 1983.

Hocking, W. K., Recent advances in radar instrumentation and techniques for studies of the mesosphere, stratosphere, and troposphere, *Radio Sci.*, *32*, 2241–2270, 1997.

Hocking, W. K., S. Fukao, T. Tsuda, M. Yamamoto, T. Sato, and S. Kato, Aspect sensitivity of stratospheric VHF radio wave scatterers particularly above 15-km altitude, *Radio Sci.*, *25*, 613–627, 1990.

Hooper, D. A., and L. Thomas, Complementary criteria for identifying regions of intense atmospheric turbulence using lower VHF radar, *J. Atmos. Sol. Terr. Phys.*, *60*, 49–61, 1998.

Ierkic, H. M., R. F. Woodman, and P. Perillat, Ultrahigh vertical resolution radar measurements in the lower stratosphere at arecibo, *Radio Sci.*, *25*, 941–952, 1990.

Kudeki, E., and R. Stitt, Frequency domain interferometry: A high resolution radar technique for studies of atmospheric turbulence, *Geophys. Res. Lett.*, *14*, 198–201, 1987.

Kudeki, E., and R. Stitt, Frequency domain interferometry studies of mesospheric layers at Jicamarca, *Radio Sci.*, *25*, 575–590, 1990.

Luce, H., M. Crochet, F. Dalaudier, and C. Sidi, Interpretation of VHF ST radar echoes from in situ temperature sheet observations, *Radio Sci.*, *30*, 1003–1025, 1995.

Muschinski, A., Turbulence and gravity waves in the vicinity of a midtropospheric warm front: A case study using VHF echo-intensity measurements and radiosonde data, *Radio Sci.*, *32*, 1161–1178, 1997.

Muschinski, A., and C. Wode, First in situ evidence for coexisting submeter temperature and humidity sheets in the lower free troposphere, *J. Atmos. Sci.*, *55*, 2893–2906, 1998.

Muschinski, A., P. B. Chilson, S. Kern, J. Nielinger, G. Schmidt, and T. Prenosil, First frequency-domain interferometry observations of large-scale vertical motion in the atmosphere, *J. Atmos. Sci.*, *56*, 1248–1258, 1999.

Muschinski, A., P. B. Chilson, R. D. Palmer, G. Schmidt, and H. Steinhagen, Boundary-layer convection and diurnal variation of vertical-velocity characteristics in the free troposphere, *Quart. J. Roy. Meteorol. Soc.*, *127*, 423–443, 2001.

Nastrom, G. D., and F. D. Eaton, Turbulence eddy dissipation rates from radar observations at 5-20 km at White Sands Missile Range, NM, *J. Geophys. Res.*, *102*, 19,495–19,505, 1997.

Ottersten, H., Mean vertical gradient of potential refractive index in turbulent mixing and radar detection of CAT, *Radio Sci.*, *4*, 1247–1249, 1969.

Palmer, R. D., R. F. Woodman, S. Fukao, M. F. Larsen, M. Yamamoto, T. Tsuda, and S. Kato, Frequency domain interferometry observations of tropo/stratospheric scattering layers using the MU radar: Description and first results, *Geophys. Res. Lett.*, *17*, 2189–2192, 1990.

Palmer, R. D., T.-Y. Yu, and P. B. Chilson, Radio imaging using frequency diversity, *Radio Sci.*, *34*, 1485–1496, 1999.

Palmer, R. D., P. B. Chilson, A. Muschinski, G. Schmidt, T.-Y. Yu, and H. Steinhagen, SOMARE 99: Observations of tropospheric scattering layers using multiple-frequency range imaging, *Radio Sci.*, this issue.

Richter, J. H., High resolution tropospheric radar soundings, *Radio Sci.*, *4*, 1261–1268, 1969.

Röttger, J., Reflection and scattering of VHF radar signals from atmospheric refactivity structures, *Radio Sci.*, *15*, 259–276, 1980.

Rüster, R., G. D. Nastrom, and G. Schmidt, High-resolution VHF radar measurements in the troposphere with a vertically pointing beam, *J. Appl. Meteorol.*, *37*, 1522–1529, 1998.

Sato, T., and R. F. Woodman, Altitude smearing due to instrumental resolution in MST radar measurements, *Geophys. Res. Lett.*, *9*, 72–75, 1982.

Schmidt, G., R. Rüster, and P. Czechowsky, Complimentary code and digital filtering for detection of weak VHF radar signals from the mesosphere, *IEEE Trans. Geosci. Electron.*, *GE-17*, 154–161, 1979.

Stitt, G. R., and S. A. Bowhill, Improving range resolution with a frequency hopping technique, in *Handbook for MAP*, edited by B. Edwards, vol. 20, pp. 448–457, SCOSTEP Secr., Univ. of Ill., Urbana, 1987.

Tatarskii, V. I., *Wave Propagation in a Turbulent Medium*, McGraw-Hill, New York, 1961.

Tsuda, T., P. T. May, T. Sato, S. Kato, and S. Fukao, Simultaneous observations of reflection echoes and refractive index gradient in the troposphere and lower stratosphere, *Radio Sci.*, *23*, 655–665, 1988.

Yoe, J. G., P. Czechowsky, R. Rüster, and G. Schmidt, Spatial variability of the aspect sensitivity of VHF radar echoes in the troposphere and lower stratosphere during jet stream passages, *Ann. Geophys.*, *12*, 733–745, 1994.

P B. Chilson and A. Muschinski, NOAA Environmental Technology Laboratory, Cooperative Institute for Research in Environmental Sciences (CIRES), University of Colorado-NOAA, 325 Broadway, R/ET2, Boulder, CO 80305-3328. (phillip.chilson@noaa.gov; andreas.muschinski@noaa.gov)

D. A. Hooper, MRI Atmospheric Research Programme, Swedish Institute of Space Physics, Box 812, S-981 28 Kiruna, Sweden. (david.hooper@irf.se)

R. D. Palmer, Department of Electrical Engineering, University of Nebraska, Lincoln, NE 68588-0511, USA. (bpalmer@unl.edu)

G. Schmidt, Max-Planck-Institut für Aeronomie, Postfach 20, D-37189 Katlenburg-Lindau, Germany. (gschmidt@linax1.mpae.gwdg.de)

H. Steinhagen, Deutscher Wetterdienst, Meteorologisches Observatorium Lindenberg, Am Observatorium 12, D-15864 Lindenberg, Germany. (hans.steinhagen@dwd.de)

(Received December 21, 1999; revised July 10, 2000; accepted September 11, 2000.)